

Neuronal SIRT3 Deletion Predisposes to Female-Specific Alterations in Cellular Metabolism, Memory, and Network Excitability

Jennifer N. Pearson-Smith,^{1,2} Ruth Fulton,¹ Christopher Q. Huynh,¹ Anna G. Figueroa,¹ Gia B. Huynh,¹ Li-Ping Liang,¹ Lindsey B. Gano,¹ Cole R. Michel,¹ Nichole Reisdorph,¹ Richard Reisdorph,¹ Kristofer S. Fritz,¹ Eric Verdin,³ and Manisha Patel¹

¹School of Pharmacy and Pharmaceutical Sciences, University of Colorado Anschutz Medical Campus, Aurora, Colorado 80045, ²Division of Geriatric Medicine, University of Colorado Anschutz Medical Campus, Aurora, Colorado 80045, and ³Buck Institute for Aging, Novato, California 94945

Mitochondrial dysfunction is an early event in the pathogenesis of neurologic disorders and aging. Sirtuin 3 (SIRT3) regulates mitochondrial function in response to the cellular environment through the reversible deacetylation of proteins involved in metabolism and reactive oxygen species detoxification. As the primary mitochondrial deacetylase, germline, or peripheral tissue-specific deletion of SIRT3 produces mitochondrial hyperacetylation and the accelerated development of age-related diseases. Given the unique metabolic demands of neurons, the role of SIRT3 in the brain is only beginning to emerge. Using mass spectrometry-based acetylomics, high-resolution respirometry, video-EEG, and cognition testing, we report targeted deletion of SIRT3 from select neurons in the cortex and hippocampus produces altered neuronal excitability and metabolic dysfunction in female mice. Targeted deletion of SIRT3 from neuronal helix-loop-helix 1 (NEX)-expressing neurons resulted in mitochondrial hyperacetylation, female-specific superoxide dismutase-2 (SOD2) modification, increased steady-state superoxide levels, metabolic reprogramming, altered neuronal excitability, and working spatial memory deficits. Inducible neuronal deletion of SIRT3 likewise produced female-specific deficits in spatial working memory. Together, the data demonstrate that deletion of SIRT3 from forebrain neurons selectively predisposes female mice to deficits in mitochondrial and cognitive function.

Key words: acetylation; cognition; excitability; female; mitochondria; sirtuin

Significance Statement

Mitochondrial SIRT3 is an enzyme shown to regulate energy metabolism and antioxidant function, by direct deacetylation of proteins. In this study, we show that neuronal SIRT3 deficiency renders female mice selectively vulnerable to impairment in redox and metabolic function, spatial memory, and neuronal excitability. The observed sex-specific effects on cognition and neuronal excitability in female SIRT3-deficient mice suggest that mitochondrial dysfunction may be one factor underlying comorbid neuronal diseases, such as Alzheimer's disease and epilepsy. Furthermore, the data suggest that SIRT3 dysfunction may predispose females to age-related metabolic and cognitive impairment.

Received June 20, 2022; revised Jan. 14, 2023; accepted Feb. 1, 2023.

Author contributions: J.N.P.-S., R.F., C.Q.H., A.G.F., L.B.G., C.R.M., N.R., R.R., K.S.F., E.V., and M.P. designed research; J.N.P.-S., R.F., C.Q.H., A.G.F., G.B.H., L.-P.L., C.R.M., N.R., R.R., and K.S.F. performed research; J.N.P.-S., R.F., C.Q.H., A.G.F., G.B.H., L.-P.L., L.B.G., C.R.M., N.R., R.R., K.S.F., and M.P. analyzed data; J.N.P.-S. and R.F. wrote the first draft of the paper; J.N.P.-S., R.F., A.G.F., G.B.H., and M.P. edited the paper; J.N.P.-S., R.F., A.G.F., G.B.H., and M.P. wrote the paper; E.V. and M.P. contributed unpublished reagents/analytic tools.

This work was supported by the following grants: National Institute of Health R37NS039587 (to M.P.), National Institute of Health R01NS039587S1 (to M.P. and J.N.P.-S.), National Institute of Health R01NS086423 (to M.P.), American Epilepsy Society Postdoctoral Fellowship (to L.B.G.), National Research Service Award NRSA F32NS090808 (to L.B.G.), and National Institute of Health T32 AG000279 (to J.N.P.-S.). Behavioral and EEG studies were performed in conjunction with the Behavior and In Vivo Neurophysiology Core, a member of the NeuroTechnology Center at the University of Colorado-School of Medicine, funded in part by the National Institute of Neurological Disorders and Stroke of the National Institutes of Health Award P30NS048154. Assistance with genomic analysis was provided by the University of Colorado-School of Medicine

Bioinformatics and Biostatistics Shared Resource Core supported by the National Institutes of Health P30CA046934. The Graduate Experience for Multicultural Students Program was supported by National Institutes of Health Grant 1R25HL 103286-08. Imaging was performed in the Advanced Light Microscopy Core Facility of the NeuroTechnology Center at the University of Colorado Anschutz Medical Campus, which is supported in part by Rocky Mountain Neurological Disorders Core Grant P30 NS048154 and by Diabetes Research Center Grant P30 DK116073. We thank Robert Valdez and Timothy Corrigan for technical assistance with EEG implantation; Katrina Diener for her technical support with acetylomics and Elizabeth Kaye (University of Colorado Anschutz Medical Campus Advanced Light Microscopy Core) for confocal imaging assistance.

The authors declare no competing financial interests.

Correspondence should be addressed to Manisha Patel at Manisha.patel@cuanschutz.edu.

<https://doi.org/10.1523/JNEUROSCI.1259-22.2023>

Copyright © 2023 the authors

Introduction

Aging is an inevitable process that is modulated by various internal and external factors, including biological sex (Austad, 2011). Sirtuin 3 (SIRT3) is gaining attention as one such modulator of cellular aging and has been shown to regulate lifespan in model organisms, such as yeast and worm (Kaeberlein et al., 1999). In humans, SIRT3 is associated with increased longevity in men and increased hormone receptor-positive breast cancer in women, suggesting a role for SIRT3 in human aging that may differ according to biological sex (Rose et al., 2003; Bellizzi et al., 2005, 2007). Curiously, despite its importance in regulating global mitochondrial function, germline deletion of *sirt3* produces no overt phenotype, although its deficiency is associated with the accelerated development of age-related diseases, such as cancer, cardiovascular disease, and metabolic diseases (Hirschey et al., 2011). Additionally, SIRT3 levels are altered in postmortem tissue obtained from patients with Alzheimer's disease (AD) and Parkinson's disease and decrease as a function of age, suggesting a potential role for SIRT3 in neurologic disease (Flurkey et al., 2007; Joseph et al., 2012; Weir et al., 2012; Shi et al., 2017; Yin et al., 2018; Pukhalskaia et al., 2020).

Reversible mitochondrial protein acetylation is a dynamic post-translational modification (PTM) that regulates mitochondrial function at multiple levels. Acetylation is a largely inhibitory PTM that is particularly enriched in mitochondria (Kim et al., 2006; Verdin and Ott, 2015). The high concentration of acetyl-CoA and basic pH within mitochondria favors an environment for nonenzymatic acetylation of susceptible proteins (Garland et al., 1965; Wagner et al., 2017). SIRT3 is a member of the highly conserved sirtuin superfamily (SIRT1–7) and one of three sirtuins localized to the mitochondria where it acts as the primary deacetylase (Onyango et al., 2002; Lombard et al., 2007). Its deacetylase activity is dependent on NAD⁺, linking SIRT3 function to the metabolic status of the cell (Finnin et al., 2001). With a broad range of target proteins involved in antioxidant response, oxidative phosphorylation (OXPHOS), the tricarboxylic acid (TCA) cycle, and fatty acid oxidation, SIRT3 is therefore postulated to be a critical, redox-sensitive interface between cellular environment and metabolism (Kumar and Lombard, 2015; Yang et al., 2016). In postmitotic cells, such as neurons, SIRT3 may be particularly important as mitochondrial acetylation can accumulate in an age-dependent manner potentially contributing to mitochondrial dysfunction.

Recent studies suggest that SIRT3 expression and function are tissue-dependent with brain exhibiting unique patterns of mitochondrial protein acetylation compared with liver mitochondria (Jin et al., 2009; Dittenhafer-Reed et al., 2015). This supports the role of SIRT3 as a key cellular rheostat linking metabolic processes to the energy demands of the cell. Whereas SIRT3 function in the liver has been intensively studied, its importance in the brain is only beginning to emerge. Moreover, its function in neurons which comprise a fraction of all cell types in brain but consume the majority of ATP is not well characterized (Herculano-Houzel, 2014). In the current study, we sought to determine the specific role of neuronal SIRT3 by selectively deleting SIRT3 in principal neurons within the hippocampus and neocortex. Deletion of SIRT3 in these highly metabolically active cells resulted in hyperacetylation of SOD2, increased cortical superoxide (O₂⁻) levels, metabolic reprogramming, altered neuronal excitability, and spatial memory deficits in 12-month-old female, but

not 12-month-old male, mice. These findings reveal a novel and unique vulnerability of female mice to the loss of neuronal SIRT3 and provide a potential mechanism by which sex differences can emerge in the context of aging and neurodegenerative disease.

Materials and Methods

Reagents. All reagents were obtained from Sigma Aldrich or Fisher Scientific unless otherwise noted.

Mice. Animal studies were conducted in accordance with the National Institute of Health's *Guide for the care and use of laboratory animals* (Publication no. 80-23). All procedures were approved by the Institute Animal Care and Use Committee of the University of Colorado Anschutz Medical Campus, which is fully accredited by the American Association for the Accreditation of Laboratory Animal Care. *Sirt3* p lox C57BL/6CrSlc mice were obtained through a material transfer agreement from the University of California–San Francisco (E.V. laboratory). These mice were crossed with *NEX-Cre C57BL/6* (Goebbels et al., 2006) or the inducible *Camk2^{cre/ERT2}* mice from The Jackson Laboratory (Madison et al., 2010) to generate the heterozygous F1 generation. The offspring were intercrossed, and genotyping was performed on the F2 progeny from ear snips collected at the time of weaning. To identify the p lox copy number, PCR was performed (ABI TaqMan probe Mm01275637_g1). Individuals carrying the *NEX-Cre* insert were identified as described by Goebbels et al. (2006). All mice, including breeders, were housed in ventilated caging on a 14/10 light/dark cycle with *ad libitum* access to standard rodent chow and filtered water. Mice (6 or 12 months old, as specified) were killed by continuous inhalation of CO₂ followed by decapitation.

Tamoxifen injection. Tamoxifen (20 mg/ml) was prepared fresh, in the dark, by first dissolving in a small amount of 95% EtOH followed by corn oil. Ten- to 12-month-old male and female *Camk2^{cre/ERT2}* mice (cnSIRT3^{+/+}, cnSIRT3^{-/-}) were injected intraperitoneally with 100 mg/kg tamoxifen or vehicle daily for 5 d. Two weeks following the last injection, we verified SIRT3 knockdown in a small subset of mice by RT-PCR and identified a significant reduction in SIRT3 expression in tamoxifen-treated cnSIRT3^{-/-} mice compared with vehicle-treated cnSIRT3^{-/-} and tamoxifen-treated cnSIRT3^{+/+} (mean fold difference ± SEM: 0.55 ± 0.12, *p* = 0.0008, *n* = 6–8/group unpaired *t* test and 0.37 ± 0.07, *p* = 0.0004, *n* = 6/group unpaired *t* test, respectively). Multiple separate cohorts of mice were treated with tamoxifen or vehicle to generate sufficient numbers for behavioral testing (described below). During the tamoxifen treatment period and the following 2 weeks, all mice were monitored for health effects by daily visual inspection and weight checks. Any mouse found to have lost >10% of its body weight was immediately killed. At the conclusion of behavior testing (described below), ~4 weeks after the initiation of tamoxifen treatment, mice were killed, and cortices collected for verification of *sirt3* knockdown by RT-PCR. Mice were excluded from behavior analysis if the *sirt3* RQ value was >0.7. This resulted in the following group numbers across three cohorts: male vehicle-treated cnSIRT3^{+/+} mice = 10, male vehicle-treated cnSIRT3^{-/-} mice = 11, male tamoxifen-treated cnSIRT3^{+/+} mice = 9, male tamoxifen-treated cnSIRT3^{-/-} mice = 12, female vehicle-treated cnSIRT3^{+/+} mice = 12, female vehicle-treated cnSIRT3^{-/-} mice = 12, female tamoxifen-treated cnSIRT3^{+/+} mice = 10; female tamoxifen-treated cnSIRT3^{-/-} mice = 6. Of these eight groups, only 2 (female tamoxifen-treated cnSIRT3^{-/-} mice and male tamoxifen-treated cnSIRT3^{-/-} mice) showed significantly decreased *sirt3* expression, as expected. Thus, the remaining six groups are controls.

Estrus cycle monitoring. Estrus cycle stage was monitored daily and/or at the time of tissue collection by vaginal lavage as previously described (Au-McLean et al., 2012). Briefly, vaginal cells were collected in ddH₂O, slide prepped, and visualized using cresyl violet stain. Cycle stage was determined as estrus when cells were comprised of mostly cornified squamous epithelial cells, proestrus when nucleated epithelial cells were predominant, and diestrus was determined when mainly leukocytes were present. For the mitochondrial protein acetylation experiment, estrus cycle in 6-month-old mice was balanced across groups or

specifically stratified for diestrus. Indeed, by stratifying female samples for diestrus or using sample sizes large enough to encompass all estrus phases, it is highly unlikely that the observed sex differences could be directly attributed to differences in circulating hormones. Moreover, SIRT3 was selectively deleted in a subset of neurons likely precluding any potential alterations to total cortical estrogen/hormone signaling.

Primary cortical cultures. Mixed cortical cell cultures were established from male and female nSIRT3^{-/-} and nSIRT3^{+/+} postnatal day 1–3 mice. Tail snips from tattooed littermates were collected and genotyped within 1 d of birth. Pups were killed and cortices dissected and placed in sterile HBSS + 10 mM HEPES. Tissue was minced finely with micro scissors, then trypsinized in a 1% solution of trypsin/HBSS for 25 min at 37°. Cells were rinsed with HBSS and triturated in a 1% solution of MEM and DNase (Sigma) until homogeneous. Cells were pelleted by centrifugation at 800 rpm for 10 min, followed by resuspension in NeuroCult plating medium (STEMCELL Technologies). Cells were then plated in PDL-treated 96 well XF96 cell culture microplates (cell density: 60,000/well; Agilent Technologies) or 48 well multielectrode array (MEA) cell culture plates (cell density: 50,000/well; Axion BioSystems) and maintained at 37°C, 5% CO₂/95% room air. After 5 DIV, one-half of the plating medium was replaced with BrainPhys neuronal medium (STEMCELL Technologies). Downstream applications are described below.

Immunocytochemistry. To validate the maturity of synapses, we performed immunocytochemistry on DIV 9 mixed cortical cells. Cells were fixed in 4% PFA and subsequently blocked for 1 h at room temperature (0.5% BSA, 2% NGS, 0.005% Tween-20, 0.05% Triton X-100). Primary antibody was applied overnight at 4°C (guinea pig anti-NeuN, Millipore N90, 1:100; rabbit anti-Synapsin I, Abcam ab254349, 1:100). Following rinses with PBS (3 × 5 min) and secondary antibody incubation at room temperature for 1 h (goat anti-guinea pig AlexaFluor 488, Invitrogen A11073, 1:100; goat anti-rabbit ATTO 647, Rockland 611-156-122, 1:100), cells were rinsed with PBS (3 × 5 min) and mounted with Prolong Diamond Antifade Mountant (Fisher Scientific). Images were captured on an Olympus FV-1000 confocal microscope with a 60× objective (Shinjuku).

MEA recordings. MEA recordings (Axion BioSystems) were performed as previously described (McConnell et al., 2012). Briefly, spontaneous network activity was measured in DIV 9 cortical cultures grown in MEA plates equipped with 16 embedded nanoporous platinum electrodes (130 μm diameter, 200 μm center-to-center spacing; Axion BioSystems) at a density of 50,000 cells/well. Data acquisition for all 768 channels was performed by Axion's Integrated Studio (AxIS 2.1.1) software, at a sampling rate of 12.5 kHz/channel and 1200 × gain. Culture viability was evaluated by monitoring spontaneous network activity at DIV 5–8. Synapse maturity at DIV 9 is illustrated in Extended Data Figure 5-1. Wells showing no spontaneous activity were excluded from analysis. Spontaneous network activity was measured as total number of spikes (variable threshold spike threshold detector set at 8 × SDs of the rms noise of each channel, bandpass filter: high pass 300 Hz, low pass 5000 Hz). Studies were performed at 37°C.

Bioenergetic profiling in male and female, nSIRT3^{-/-} and nSIRT3^{+/+} cultures. Mitochondrial respiration and extracellular glycolytic parameters were investigated in primary mixed neuronal glial cultures at DIV 8 using a Seahorse XFe96 Analyzer (Agilent BioSciences) following standard protocols (Pelletier et al., 2014). On the day of the experiment, cell culture media was exchanged for glucose and serum-free XF assay media and plates (60,000 cells/well) were transferred to a 37°C, CO₂-free incubator for 1 h before measurement. Real-time extracellular acidification rate was measured 3 times under baseline conditions and following the acute injection of glucose (16 mM), oligomycin (1 μM), and 2-deoxyglucose (50 mM). Basal oxygen consumption rates were obtained before glucose injection. Values were normalized to protein amount as determined by Bradford Assay (Fisher Scientific).

Mitochondrial isolation. Crude mitochondria were obtained from the forebrain (cortex and hippocampus) of adult mice as previously described (Liang and Patel, 2006). Briefly, ice-cold brain homogenates were centrifuged for 10 min at 3000 × g (4°C), and the resulting

supernatant was centrifuged for another 10 min at 13,000 × g (4°C). Mitochondrial pellets were stored at –80°C for future use.

Immunoblotting. To assess protein expression, cortical tissue or mitochondria from 6- and 12-month-old mice were lysed in SDS buffer and protein yield was determined by Bradford Assay (Fisher Scientific). Samples were diluted in PBS, combined with Laemmli sample buffer (2.5% β mercaptoethanol [1:1], Bio-Rad), heated to 95°C for 10 min, and placed on ice. Criterion stain-free gels (4%–20%) were then loaded with 25 μg protein and electrophoresed for 1 h at 200 V in 1 × Tris/glycine/SDS buffer (Bio-Rad). Protein was transferred to PVDF membranes on a Trans-blot turbo transfer system following the manufacturer's instructions (Bio-Rad) and then blocked for 1 h in 5% milk and TBST (0.1% Tween). Membrane was incubated with primary antibody overnight at 4°C (SOD2 ab13534, Abcam, 1:200; SOD2 K68 ab137037, Abcam, 1:200; SOD2 K122 ab214675, Abcam, 1:200; acetyl-lysine 9814, Cell Signaling, 1:1000; acetyl-lysine ICP0380, Immunechem Pharmaceuticals, 1:200; SIRT3 5490, Cell Signaling, 1:200) followed by secondary antibody (HRP-conjugated goat rabbit, Invitrogen 31460) at 1:10,000 concentration for 1 h. Selection of primary antibodies was based on peer-reviewed reports that illustrate validation using *in vitro* acetylation treatment (Assiri et al., 2017; Gano et al., 2018). The membrane was developed with SuperSignal West Pico PLUS Chemiluminescent substrate (Fisher Scientific) and imaged for both total protein and HRP signal on a Bio-Rad ChemiDoc MP imaging system. The HRP signal was quantified using ImageLab 6.0.1 software (Bio-Rad) and normalized to the total protein signal.

Mass spectrometry-based acetylomics. Cortical mitochondria were isolated from 12-month-old male and female nSIRT3^{-/-} and nSIRT3^{+/+} mice (6/group = 24 total mice) as described above for acetylomics analysis. To have enough protein for analysis, mitochondria were pooled from 2 mice of the same sex and genotype to form one sample. Analysis was then performed on three samples/group. Sample preparation, data collection, accurate mass and retention time (AMRT) library generation, and data analysis were performed as previously described (Ali et al., 2019). A total of 3.2 mg from each pooled sample was spiked with 75 ng of acetylated whole protein BSA and trypsin-digested overnight, acidified with TFA, purified using Sep-Pak C18 Classic Cartridges (Waters, #WAT051910), frozen at –80°C for 4 h, and lyophilized for 48 h. Samples were incubated 2 h at 4°C with immunoaffinity beads conjugated to acetyl lysine antibody (PTMScan Acetyl-Lysine Motif [Ac-K] Immunoaffinity Beads (#13416, Cell Signaling). After incubation, the supernatants were collected and the remaining beads were washed with IAP buffer twice (PTM Scan IAP Buffer 9993, Cell Signaling) and with Burdick and Jackson LC-MS grade water 3 times (Honeywell). Peptides were eluted with 0.15% TFA twice, pooled, cleaned by Pierce C18 Spin Tips (Fisher Scientific, #84850), evaporated to dryness, and frozen at –80°C. Dried samples were resuspended in 15 fmol/μl of PROCAL Retention Time Standard Kit peptides (JPT Peptide Technologies, #RTK-1 10 pmol) in 3% ACN, 0.1% formic acid in water for LC-MS and LC-MS/MS analysis.

Enriched acetyl lysine peptides were loaded to a 2 cm PepMap 100, nanoviper trapping column and resolved online using a 0.075 × 250 mm, 2.0 μm Acclaim PepMap RSLC reverse-phase nano column (Fisher Scientific) by 1290 Infinity II LC system with a nanoadapter (Agilent Technologies). Mobile phases consisted of water + 0.1% formic acid (A) and 90% aqueous acetonitrile + 0.1% formic acid (B). Samples were loaded onto the trapping column at 3.2 μl/min for 3.5 min before separation via flow rate of 330 nl/min and a gradient of 3%–7% B over 2 min, 7%–35% B over 43 min, and 35%–70% B over 2 min for a 47 min gradient at 42°C. The column wash was performed at 70% B for 5 min. Data were acquired using a 6550 Q-TOF with a nano source (Agilent Technologies) operated in MS-Only mode for peptide quantification for every sample or pooled samples of nSIRT3^{-/-} and nSIRT3^{+/+} female and male groups. Analysis was performed using intensity-dependent CID MS/MS for peptide identifications. Capillary voltage, drying gas flow, and drying gas temperature were 1300 V, 11.0 L/min, and 175°C, respectively. MS/MS data were collected using positive ion polarity at mass ranges 260–1700 m/z and a scan rate of 6 spectra/s for MS scans and mass ranges 50–1700 m/z at a scan rate of 3 spectra/s for MS/MS scans. All charge states, excluding singly charged species, were included for MS/MS acquisition, and

preference was given for charge States 2 and 3. MS-only analysis was performed at a fixed scan rate of 1.5 spectra/s.

We used SpectrumMill software (Agilent Technologies) to extract, search, and review peptide identities. The SwissProt Mus Musculus database allowing up to four missed tryptic cleavages and fixed carbamidomethyl (C) and variable deamidated (NQ), oxidation (M), and acetylation (K) modifications. Monoisotopic mass tolerance allowed was ± 20.0 ppm and the MS/MS tolerance was ± 50 ppm. Acetylated peptides having a minimum peptide score of 8 and scored peak intensity of 50% were included in building the AMRT library.

LC-MS quantitative data were extracted and aligned with Profinder V.B.10.00 software (Agilent Technologies). Retention times, neutral masses, and chemical formulas identified in the AMRT library were used for batched feature extractions; for extraction, an ion count threshold of 2 or more ions and 8000 counts along with score threshold of 50. Scoring includes MS quality, isotope abundance, and isotope spacing that match to a targeted chemical formula in a given retention time window in the AMRT library. Charge States 2–6 were included with H^+ adducts. Mass window alignment and retention time tolerances were set to 10 ppm and 0.8 m, respectively. The extraction and alignment data were quantified using Mass Profiler Professional version 14.9 (Agilent Technologies). Acetylated BSA peptides were used to assess the variance in sample preparation between samples. Overall, internal standards used in our approach accounted for acetyl peptide enrichment, sample injection, and chromatographic retention. Based on rigorous PROCAL and acetyl-BSA standardization, acetyl peptide identifications acquired from 0–33 min were included from both sexes for bioinformatics analysis.

Statistical analysis included peptides found in 100% of 1 of 4 conditions for group-to-group comparisons. Volcano plots of acetyl peptides were generated using a moderated *t* test for peptides with a fold change ≤ 2.0 or ≥ 2.0 and a Benjamini-Hochberg multiple-testing correction *p* value < 0.05 . A two-way ANOVA between genotypes and sex was performed to determine the overall effects of genetic differences versus sex differences at various lysine acetylation sites.

Superoxide measurement. The $O_2^{\cdot-}$ sensitive, 2-hydroxyethidium (2-OH- E^+) was measured by an HPLC coupled with an electrochemical detector following the method previously described with minor modifications (Zielonka et al., 2006; Maghzal and Stocker, 2007). Twelve-month-old-mice were injected with 50 mg/kg (s.c.) dihydroethidium (DHE, Sigma Aldrich #37291) and killed 1 h after injection. Brain samples were sonicated in ice-cold 0.1N PCA (0.1 g/ml, w/v) and centrifuged at $16,000 \times g$ at 4°C for 10 min. An aliquot of 20 μ l was injected into the HPLC-EC system (ESA Biosciences), which consists of two pumps (model 582), a temperature controlled autosampler (model 542), and an 8-channel electrochemical CoulArray (model 5600) detector set to the potentials 0, 200, 280, 365, 400, 450, 500, and 600 mV versus the palladium reference electrode. The mobile phase contained 50 mM PB, pH 2.6, 2% acetonitrile. HE, 2-OH- E^+ , and E^+ were separated on a Phenomenex Polar-RP 80 A column (4 μ m, 250 \times 4.6 mm; Phenomenex). The flow rate was 0.6 ml/min, and the pressure was ~ 78 bar.

EEG analysis. Twelve-month-old-mice were anesthetized (isoflurane) and implanted with bilateral dural stainless-steel electrodes (Pinnacle Technology; AP: -0.5 mm from bregma, ML: ± 2.0 mm from midline). Two additional electrodes positioned near the lambdoid suture on left and right hemispheres served as a reference and ground electrode. Electrodes were secured to the skull with dental acrylic. Mice received buprenorphine once daily for 2 d. After a 5 d recovery period, synchronized time-locked video and EEG signals (Pinnacle Technology) were recorded continuously for 14 d. The EEG signals were digitized at 2000 Hz with acquisition filters set at 0.5 Hz (low) and 500 Hz (high) and stored on a hard disk for offline analysis. EEG records were searched for seizure-related parameters, including interictal spikes (ISs) by an investigator blinded to animal genotype and sex. An IS was noted when a high amplitude (at least $3 \times$ baseline) sharp wave was observed. IS quantitation and power spectral plots of EEG signal were acquired using Sirenia Seizure Pro software (Pinnacle Technology).

High-resolution respirometry. To assess Complex I (CI) function, maximum mitochondrial respiratory capacity was measured pairwise in

freshly isolated cortical mitochondria from 12-month-old sex- and genotype-matched mice. Samples were compared by high-resolution respirometry (Oxygraph-2k; O2k, Oroboros Instruments) in the presence of CI and Complex II (CII) substrates according to established protocols with minor modification (Votien et al., 2012). Briefly, mitochondria were isolated as described above in mitochondrial isolation buffer A (320 mM sucrose, 10 mM Tris-Cl, 1 mM K^+ EDTA, 2.5 g/l BSA, pH 7.4). Mitochondria were resuspended in respiration buffer (MiR05) and loaded into a previously oxygenated (200 mM catalase and 200 mM H_2O_2), oxygraph chamber at 37°C. After the addition of mitochondria, the following compounds were added to the oxygraph: 10 mM glutamate, 2 mM malate, 5 mM pyruvate, 5 mM ADP, 10 μ M cytochrome C, 10 mM succinate, 0.5 μ M FCCP, 0.5 μ M rotenone, and 2.5 μ M antimycin A. After each injection of substrate, uncoupler, or inhibitor (SUIT-011D024), a 5-point averaging window was used to determine the oxygen consumption from the change in concentration of oxygen within the chamber.

Enzyme activity assays. SOD2 enzyme activity was measured by colorimetric detection of formazan dye following production of $O_2^{\cdot-}$ via xanthine oxidase in 12-month-old-mice (Sun et al., 1988). Mitochondria were isolated from cortical tissue by homogenizing in cold buffer containing 20 mM HEPES, pH 7.2, 1 mM EGTA, 210 mM mannitol, and 70 mM sucrose. Samples were centrifuged first at $1500 \times g$ followed by $10,000 \times g$. Residual CuZn-SOD and EC-SOD activity was deactivated via incubation with 3 mM potassium cyanide for 30 min. SOD2 enzyme activity was then assessed with a Cayman Chemical superoxide dismutase assay kit, and 460 nm absorbance was measured on a BioTek Synergy four plate reader (Agilent Technologies). Protein normalization was performed via Coomassie Blue assay (Fisher Scientific).

NADH:ubiquinone oxidoreductase (CI) activity was measured in crude mitochondria isolated from 12-month-old-mice as previously described (Birch-Machin and Turnbull, 2001). Crude mitochondria were lysed by freeze-thawing in hypotonic buffer (25 mM KH_2PO_4 , 5 mM $MgCl_2$, pH 7.4). The reaction was initiated by the addition of 50 μ g mitochondria to the assay buffer (hypotonic buffer with 65 μ M ubiquinone, 130 μ M NADH, 2 μ g/ml antimycin A, and 2.5 mg/ml defatted BSA). The oxidation of NADH by CI was monitored spectrophotometrically at 340 nm for 2 min at 30°C. Activity was further monitored for an additional 2 min following the addition of rotenone (2 μ g/ml). The difference between the rate of oxidation before and after the addition of rotenone was used to calculate CI activity.

Aconitase and fumarase activities were measured as described previously (Patel et al., 1996). Briefly, mitochondria were isolated from cortical tissue and homogenized in 70 mM sucrose, 210 mM mannitol, 10 mM Tris HCl, 1 mM EDTA, pH 7.4. Mitochondria were isolated from the homogenate following two differential centrifugation steps ($3000 \times g$ followed by $13,000 \times g$) and snap frozen in liquid nitrogen; 50 μ l of the mitochondria was combined with either 100 μ l 200 mM isocitrate (aconitase assay) or 50 mM malate (fumarase assay) and placed in a cuvette containing 850 μ l reaction buffer (aconitase assay: 50 μ l mM Tris HCl and 600 μ M $MnCl_2$; and fumarase assay: 30 mM KH_2PO_4 , 100 μ M EDTA, pH 7.4). The rate of the conversion of *cis*-aconitate to isocitrate (aconitase assay) or fumarate to L-malate (fumarase assay) was measured spectrophotometrically by detecting the increased rate of absorbance at 240 nm. Protein normalization was performed via Coomassie Blue assay (Fisher Scientific).

Cognitive testing. Multiple cohorts of mice underwent Y-maze testing for spatial working memory at 6 or 12 months of age. Mice were acclimated to conditions approximating that of the Y-maze over several days. Specifically, mice were brought to the dedicated behavioral testing room for 2 h before returning to the housing room. The next day, mice performed an open field task as an initial assessment of locomotion and exploratory drive. The following day, test order was randomized using a random number generator (www.random.org) and mice were allowed to explore the Y-maze apparatus (arm length 30 cm) for 8 min. A successful alternation was noted on three consecutive arm entries (i.e., A-B-C), while an unsuccessful alternation was recorded when the mouse returned to the most recently explored arm (i.e.,

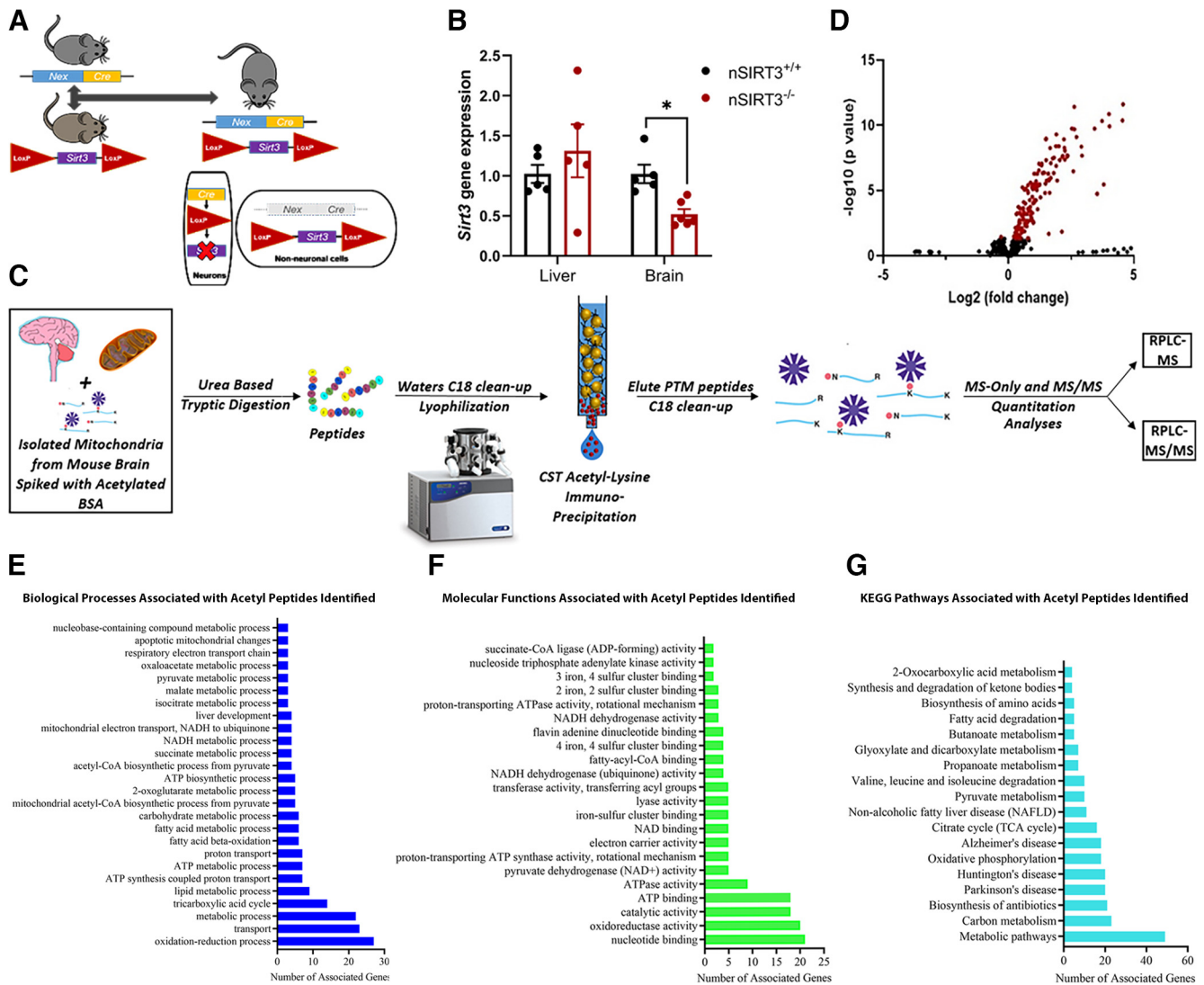


Figure 1. Targeted deletion of neuronal SIRT3 results in hyperacetylation of mitochondrial proteins. **A**, Schematic represents Cre-loxP strategy for targeting Nex to induce forebrain-specific neuronal SIRT3 deletion. **B**, *Sirt3* gene expression in liver and cortex ($n = 5$ or 6 /group). $**p < 0.01$ (unpaired t test). **C**, Mass spectrometry-based acetylotomic workflow. **D**, Volcano plot of significantly hyperacetylated (red) and unaltered (black) proteins in nSIRT3^{-/-} cortical mitochondria from 12-month-old-mice ($n = 6$ /group; Benjamini-Hochberg-corrected $p < 0.05$). Bioinformatic analysis of significantly increased acetyl peptides using DAVID (version 6.8) identified enriched pathways related to **(E)** biological processes, **(F)** molecular functions, and **(G)** KEGG pathways (fold change > 1.2). Proteins identified to have significant changes in acetylation levels are shown in Extended Data Table 1-1.

A-B-A). Total arm entries and sequence of arm entries were recorded, and percent alternation was calculated as follows: [(the number of actual alternations \div the maximum possible alternations) $\times 100$].

Statistical analysis. The distribution of data before analyses was evaluated with the Shapiro-Wilk test for normal distribution. Data meeting this criterion were compared with Student's t test and evaluated for effects of genotype and sex using two-way ANOVA. Significant main effects and interactions ($p < 0.05$) were probed using Sidak's multiple comparison test. All data are presented as mean \pm SEM unless otherwise noted. Analyses were performed using Prism 9.3.1 software (GraphPad Software).

Results

Targeted deletion of neuronal-SIRT3 results in hyperacetylation of mitochondrial proteins

To investigate the role of SIRT3 in a clinically relevant subset of neurons, *sirt3* floxed mice were crossed with the constitutive Cre line under the control of NEX, a basic helix-loop-helix protein

(Lombard et al., 2007) (Fig. 1A). This Cre-loxP approach has been previously shown to restrict target gene deletion to principal excitatory neurons of the forebrain in primarily cortical and hippocampal areas (Goebbels et al., 2006). Offspring were born in a normal Mendelian ratio and displayed no obvious physical phenotype. We verified the presence of the *sirt3* gene in liver in both nSIRT3^{+/+} and nSIRT3^{-/-} mice and an $\sim 50\%$ reduction of brain SIRT3 expression in nSIRT3^{-/-} mice (Fig. 1B), consistent with neuronal-specific KO of SIRT3. To ensure that deletion of SIRT3 from just a subset of neurons was sufficient to increase cortical mitochondrial acetylation, a direct consequence of its enzymatic function, we performed mass spectrometry-based acetylotomics in 12-month-old male and female mice (schematic represented in Fig. 1C). Using this approach in isolated cortical mitochondria, we identified 205 significantly hyperacetylated peptides corresponding to 88 different proteins in nSIRT3^{-/-} mice across gender (Fig. 1D; Extended Data Table 1-1). Further bioinformatics analysis identified pathologically

Table 1. Identity of hyperacetylated proteins involved in TCA cycle and mitochondrial electron transport in nSIRT3^{-/-} mice (n = 6 nSIRT3^{-/-} mice, n = 6 nSIRT3^{+/+} mice)

Protein	Gene	Accession no.	No. of lysine mod sites
Aconitate hydratase, mitochondrial	Aco2	Q99K10	7
ATP synthase F(0) complex subunit B1, mitochondrial	Atp5pb	Q9CQ07	1
ATP synthase protein 8	Mtstp8	P03930	1
ATP synthase subunit alpha, mitochondrial	Atp5f1a	Q03265	8
ATP synthase subunit beta, mitochondrial	Atp5f1b	P56480	6
ATP synthase subunit epsilon, mitochondrial	Atp5f1e	P56382	1
ATP synthase subunit O, mitochondrial	Atp5po	Q9DB20	3
ATP synthase-coupling factor 6, mitochondrial	Atp5pf	P97450	1
Citrate synthase, mitochondrial	Cs	Q9CZU6	8
Cytochrome c oxidase subunit 4 isoform 1, mitochondrial	Cox4i1	P19783	1
Cytochrome c1, heme protein, mitochondrial	Cyc1	Q9D0M3	1
Dihydropyridyl dehydrogenase, mitochondrial	Dld	O08749	5
Dihydropyridyllysine-residue acetyltransferase component of pyruvate dehydrogenase complex, mitochondrial	Dlat	Q8BMF4	2
Dihydropyridyllysine-residue succinyltransferase component of 2-oxoglutarate dehydrogenase complex, mitochondria	Dlst	Q9D2G2	1
Fumarate hydratase, mitochondrial	Fh	P97807	2
Hydroxyacylglutathione hydrolase, mitochondrial	Hagh	Q99KB8	1
Isocitrate dehydrogenase [NAD] subunit alpha, mitochondrial	Idh3a	Q9D6R2	6
Isocitrate dehydrogenase [NAD] subunit γ 1, mitochondrial	Idh3g	P70404	2
Malate dehydrogenase, mitochondrial	Mdh2	P08249	5
NAD-dependent malic enzyme, mitochondrial	Me2	Q99KE1	1
NADH dehydrogenase [ubiquinone] 1 alpha subcomplex subunit 2	Ndufa2	Q9CQ75	2
NADH dehydrogenase [ubiquinone] 1 alpha subcomplex subunit 7	Ndufa7	Q9Z1P6	2
NADH dehydrogenase [ubiquinone] 1 alpha subcomplex subunit 9, mitochondrial	Ndufa9	Q9DC69	2
NADH dehydrogenase [ubiquinone] 1 beta subcomplex subunit 11, mitochondrial	Ndufb11	O09111	1
NADH dehydrogenase [ubiquinone] iron-sulfur protein 6, mitochondrial	Ndufs6	P52503	1
NADH dehydrogenase [ubiquinone] iron-sulfur protein 7, mitochondrial	Ndufs7	Q9DC70	1
NADH-ubiquinone oxidoreductase 75 kDa subunit, mitochondrial	Ndufs1	Q91VD9	2
Pyruvate dehydrogenase E1 component subunit alpha, somatic form, mitochondrial	Pdha1	P35486	3
Pyruvate dehydrogenase E1 component subunit alpha, testis-specific form, mitochondrial	Pdha2	P35487	3
Pyruvate dehydrogenase protein X component, mitochondrial	Pdhx	Q8BKZ9	3
Succinate dehydrogenase [ubiquinone] flavoprotein subunit, mitochondrial	Sdha	Q8K2B3	2
Succinate dehydrogenase [ubiquinone] iron-sulfur subunit, mitochondrial	Sdhb	Q9CQA3	1
Succinate-CoA ligase [ADP/GDP-forming] subunit alpha, mitochondrial	Suclg1	Q9WUM5	7
Succinate-CoA ligase [ADP-forming] subunit beta, mitochondrial	Sucla2	Q9Z219	3

relevant pathways enriched in biological processes (Fig. 1E), molecular functions (Fig. 1F), and KEGG pathways (Fig. 1G), all associated with the 88 proteins found to have significant changes in acetylation by at least a 1.2-fold increase. Most of the identified proteins were involved in metabolic processes, including the TCA cycle and oxidative processes (Fig. 1E–G; Table 1; Extended Data Table 1–1).

Neuronal-SIRT3 deficiency predisposes to mitochondrial hyperacetylation but not enzymatic dysfunction

We sought to characterize any potential sex differences in these mice by directly comparing acetylation levels with SDS page and immunoblotting. We first verified that mitochondrial SIRT3 protein levels were equivalent between the sexes and its deficiency in 12-month-old nSIRT3^{-/-} mice (Fig. 2A). Using acetyl-lysine antibodies, we found global mitochondrial acetylation to be significantly increased in both male and female nSIRT3^{-/-} mice at 6 months (Fig. 2B) and 12 months of age (Fig. 2C). We rationalized that if circulating hormones such as estrogen or progesterone were sufficient to increase brain mitochondrial acetylation, this would be reflected in the hormonal fluctuations associated with estrus cycle. To determine whether hormonal fluctuations associated with estrus cycle would increase brain mitochondrial acetylation, we assessed mitochondrial pan-acetylation in female mice at 6 months of age staged in proestrus, estrus, or diestrus. Regardless of estrus

stage, nSIRT3^{-/-} mice exhibited significantly increased acetylation relative to nSIRT3^{+/+} mice (Fig. 2D).

As a major target of SIRT3-mediated deacetylation, multiple subunits of CI were hyperacetylated in nSIRT3^{-/-} mice (Table 1). Among these were core subunits comprising the minimal assembly required for catalysis, including the 75 kDa subunit (*Ndufs1*) which was acetylated at two lysine sites, K68 and K122 (Table 1). We sought to identify the enzymatic effect of these findings by examining CI activity in 12-month-old mice. Interestingly, CI activity was unaffected in nSIRT3^{-/-} mice relative to nSIRT3^{+/+} (Fig. 2E). Moreover, hyperacetylation at multiple sites of mitochondrial aconitase (Table 1; Fig. 2F) and fumarase (Fig. 2G) was not sufficient to alter the activities of these TCA cycle enzymes. Together, this suggests that deletion of SIRT3 is sufficient to induce cortical mitochondrial protein hyperacetylation; however, this hyperacetylation does not appear to influence downstream enzymatic function of specific target proteins.

Neuronal-SIRT3 deficiency results in sex-specific alterations to SOD2

SOD2, a critical target of SIRT3-mediated deacetylation, is the primary enzyme capable of detoxifying mitochondrial O₂⁻; and inhibition of its activity by hyperacetylation leads to mitochondrial oxidative stress (Qiu et al., 2010; Tao et al., 2010; Chen et al., 2011; Dikalova et al., 2017). Given that global mitochondrial protein acetylation was significantly increased in nSIRT3^{-/-}

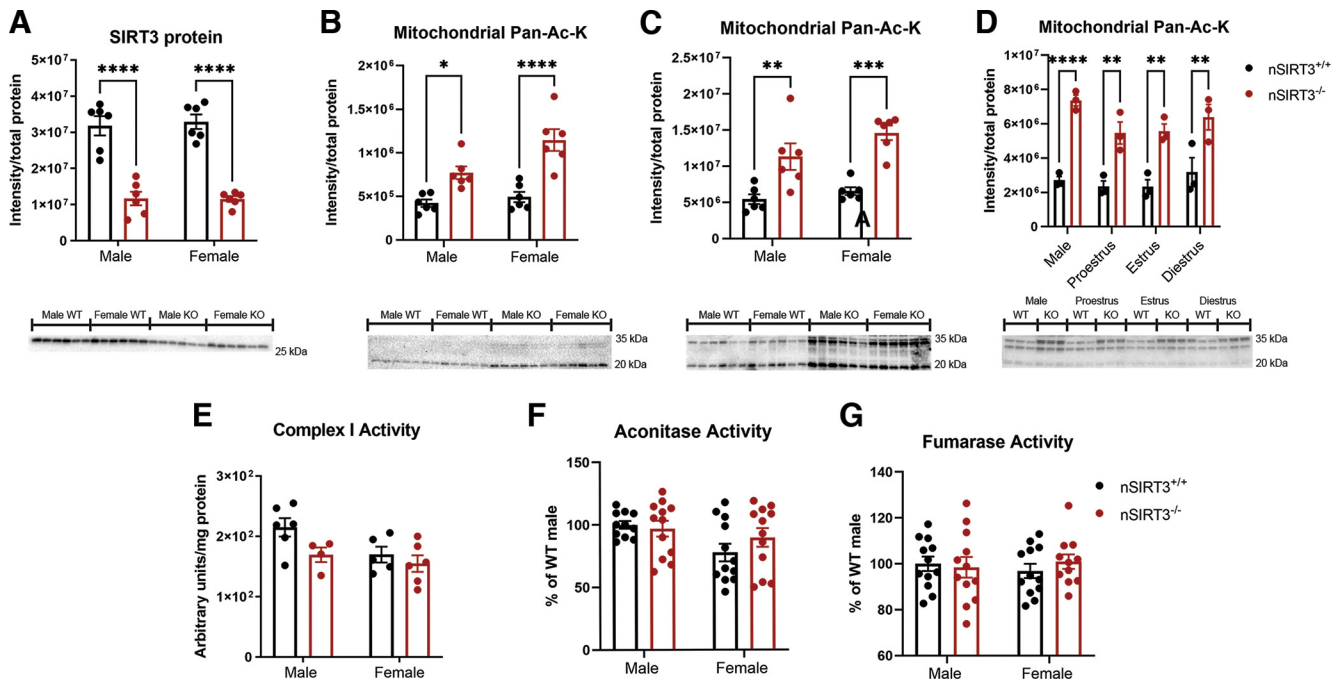


Figure 2. Neuronal SIRT3 deficiency predisposes to mitochondrial hyperacetylation but not enzymatic dysfunction. Western blot and band densitometry analysis of (A) SIRT3 in cortical mitochondrial isolates ($n = 6/\text{group}$), total mitochondrial protein acetylation levels in cortical mitochondrial isolates in (B) 6-month-old and (C) 12-month-old-mice ($n = 6/\text{group}$), and of total mitochondrial protein acetylation levels across estrus cycle in 6-month-old female mice and male mice ($n = 3/\text{group}$) (D). Protein expression and protein acetylation levels were normalized to total protein load. Enzymatic activity in 12-month-old mice (E) CI activity ($n = 4\text{--}6/\text{group}$), (F) aconitase activity ($n = 11$ or $12/\text{group}$), and (G) fumarase activity ($n = 11$ or $12/\text{group}$). Total mitochondrial acetylation levels and enzymatic activity were compared by two-way ANOVA followed by Sidak's multiple comparison test. *Post hoc* significance: $*p < 0.05$; $**p < 0.01$; $***p < 0.001$; $****p < 0.0001$. Error bars indicate mean \pm SEM.

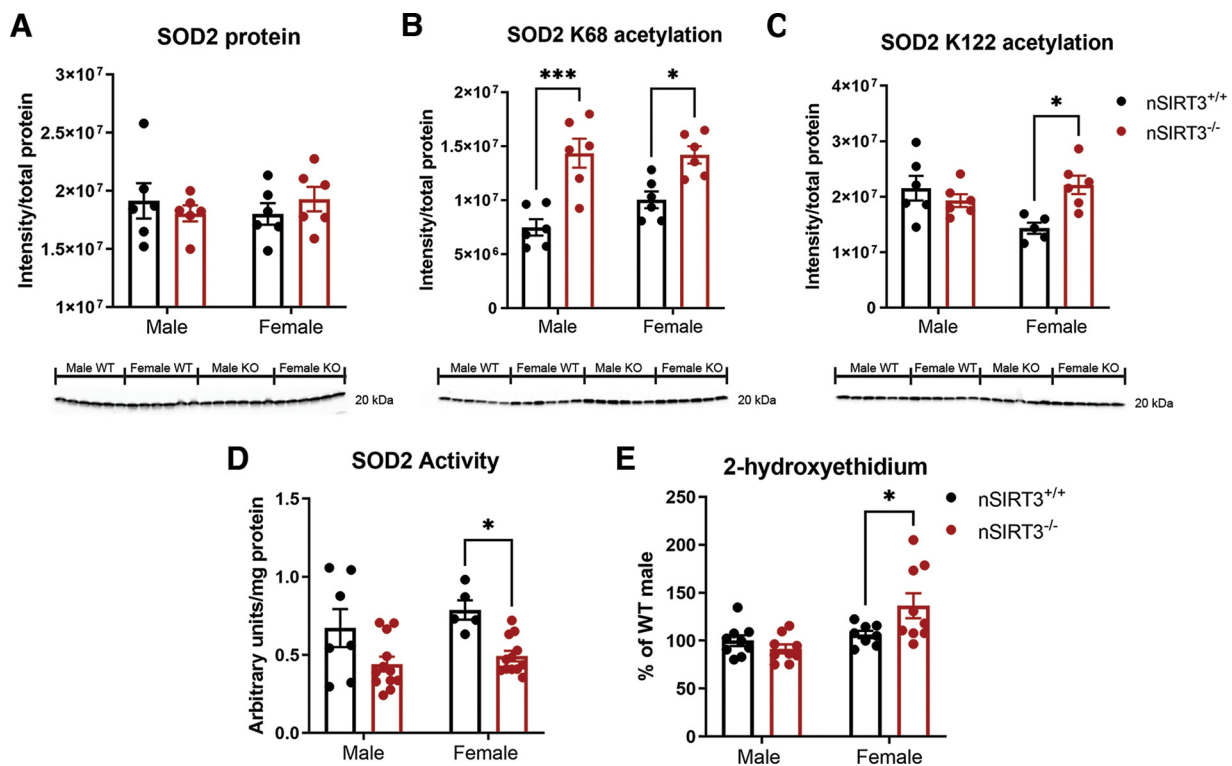


Figure 3. Neuronal SIRT3 deficiency results in sex-specific alterations to SOD2. Western blot and band densitometry analysis of (A) SOD2 in 12-month-old-mice ($n = 6/\text{group}$), (B) acetylated K68 of SOD2 in 12-month-old-mice ($n = 6/\text{group}$), and (C) acetylated K122 of SOD2 in 12-month-old-mice ($n = 6/\text{group}$). Protein expression and protein acetylation levels were normalized to total protein load. D, SOD2 activity in 12-month-old-mice ($n = 7\text{--}9/\text{group}$). E, HPLC-based detection of 2-OH-E⁺, which is generated specifically by the superoxide-derived oxidation of DHE in 12-month-old-mice ($n = 8$ or $9/\text{group}$). Data analyzed by two-way ANOVA followed by Sidak's multiple comparison test. Total mitochondrial acetylation levels and enzymatic activity were compared by two-way ANOVA followed by Sidak's multiple comparison test. *Post hoc* significance: $*p < 0.05$; $**p < 0.01$; $***p < 0.001$; $****p < 0.0001$. Error bars indicate mean \pm SEM.

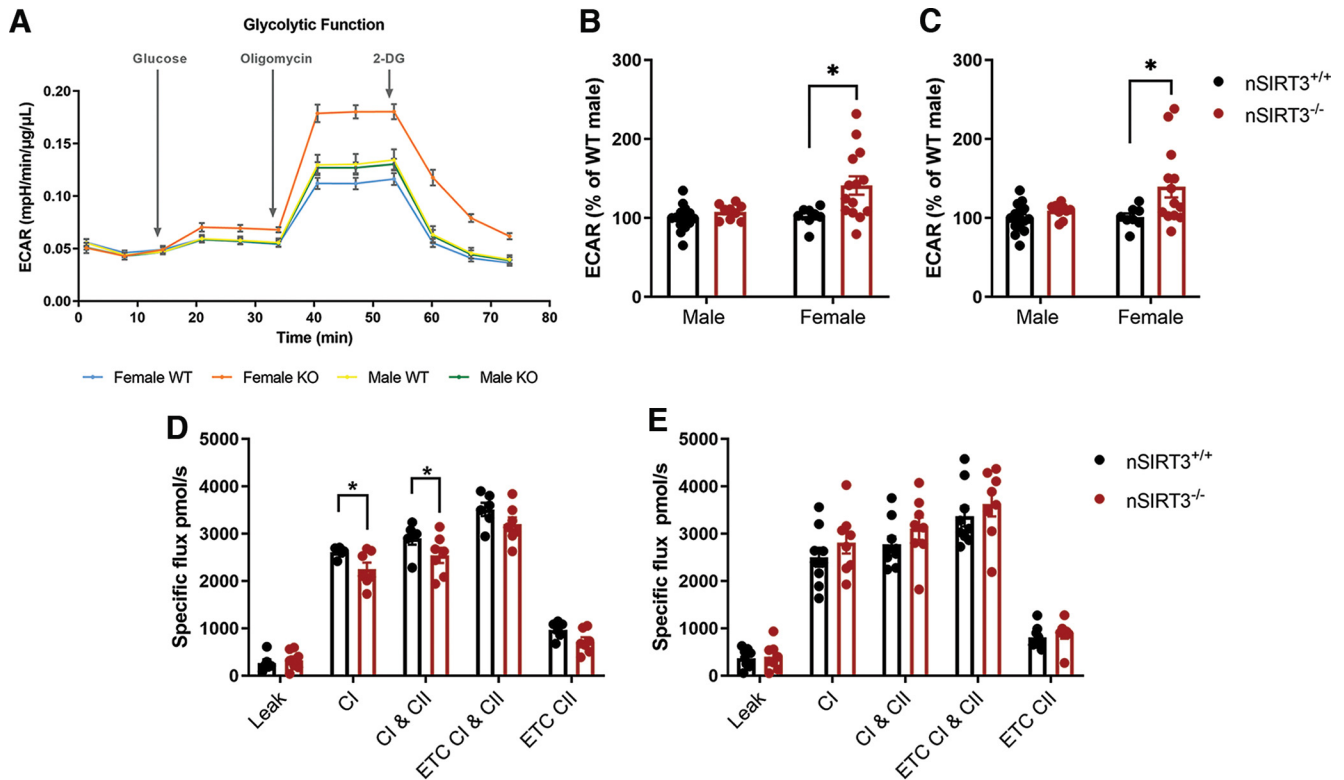


Figure 4. Neuron-specific SIRT3 deletion results in sex-specific effects on cellular metabolism. *A*, Representative image of *in vitro* extracellular acidification rate. *B*, Quantification of baseline glycolysis and (*C*) glycolytic reserve. *n* = 9–15/group (biological replicates), 10 technical replicates, across 9 total experiments. Data compared by two-way ANOVA followed by Sidak's multiple comparison test. Mitochondrial oxygen consumption compared by high resolution respirometry in the presence of CI and CII substrates and inhibitors in 12-month-old (*D*) female and (*E*) male mice (*n* = 6–10). **p* < 0.05 (multiple *t* test). Error bars indicate mean ± SEM.

mice relative to nSIRT3^{+/+} mice, we sought to determine whether SOD2 key functional lysine residues, such as K68 and K122, exhibited a similar acetylation pattern. Despite no changes in the protein levels of SOD2 (Fig. 3*A*), acetylation at K68 was significantly increased in both male and female nSIRT3^{-/-} mice relative to nSIRT3^{+/+} at 12 months of age (Fig. 3*B*). Interestingly, acetylation at K122 was only significantly elevated in female nSIRT3^{-/-} mice (Fig. 3*C*) at 12 months of age.

To determine whether differences in SOD2 K122 hyperacetylation conferred alterations to its functional capacity, we examined SOD2 activity in crude mitochondria from 12-month-old-mice. Compared with their WT controls, female nSIRT3^{-/-} mice exhibited significantly decreased SOD2 activity (Fig. 3*D*). To examine whether decreased SOD2 activity was sufficient to increase steady-state O₂⁻ levels, we assessed O₂⁻ levels in cortical tissue using HPLC-based detection of O₂⁻ sensitive 2-OH-E⁺. 2-OH-E⁺ is formed from the specific oxidation of DHE by O₂⁻ (Zhao et al., 2003, 2005; Fink et al., 2004). After peripheral injection of DHE, we detected significantly increased levels of 2-OH-E⁺ in female nSIRT3^{-/-} mice compared with female nSIRT3^{+/+} (Fig. 3*E*). Together, these data suggest that neuronal-specific SIRT3 deletion results in sex-specific hyperacetylation to SOD2 key functional lysine residue K122 and result in female-specific elevated cortical O₂⁻ levels and decreased SOD2 activity.

Neuron-specific SIRT3 deletion results in sex-specific effects on cellular metabolism

Through deacetylation of enzymes associated with various metabolic pathways, SIRT3 is capable of affecting global shifts in cellular metabolism (Finley and Haigis, 2012). We therefore sought

to investigate cellular bioenergetics using a combination of approaches. First, we determined the consequences of neuron-specific deletion of SIRT3 in primary cultured cells grown in culture (DIV 9). Real-time bio-energetic profiling of extracellular acidification rate and oxygen consumption rate allowed for measurement of glycolysis and mitochondrial respiration, respectively. Extracellular acidification rate was significantly elevated by genotype and sex such that cultures obtained from female nSIRT3^{-/-} mice exhibited increased baseline glycolysis (Fig. 4*A, B*) and glycolytic capacity (Fig. 4*A, C*) compared with all other groups. Baseline oxygen consumption rate was not different between genotypes (mean % of KO male ± SEM; 89.23 ± 7.647 for WT male, 112.3 ± 6.415 for WT female, 108.9 ± 6.415; *n* = 4–9/group).

To further assess mitochondrial bioenergetics, maximum mitochondrial respiratory capacity was measured pairwise in freshly isolated cortical mitochondria from 12-month-old sex-matched, nSIRT3^{+/+} and nSIRT3^{-/-} mice. Samples were compared by high-resolution respirometry (Oroboros, O2K) in the presence of CI and CII substrates and inhibitors. Relative to female nSIRT3^{+/+} mice, female nSIRT3^{-/-} mice exhibited significantly decreased CI-linked respiration, significantly reduced CI+CII-linked respiration, and a trend toward decreased ET capacity associated with CI+CII respiration (Fig. 4*D*). ET capacity in the presence of CI inhibitor, rotenone, was not significantly different, suggesting that these differences were driven by CI. Conversely, maximum respiratory capacity was not significantly altered in male nSIRT3^{-/-} mice (Fig. 4*E*). CI enzymatic activity was not significantly different between male and female nSIRT3^{-/-} mice (Fig. 2*E*), suggesting that decreased CI activity does not account for differences in CI oxygen consumption.

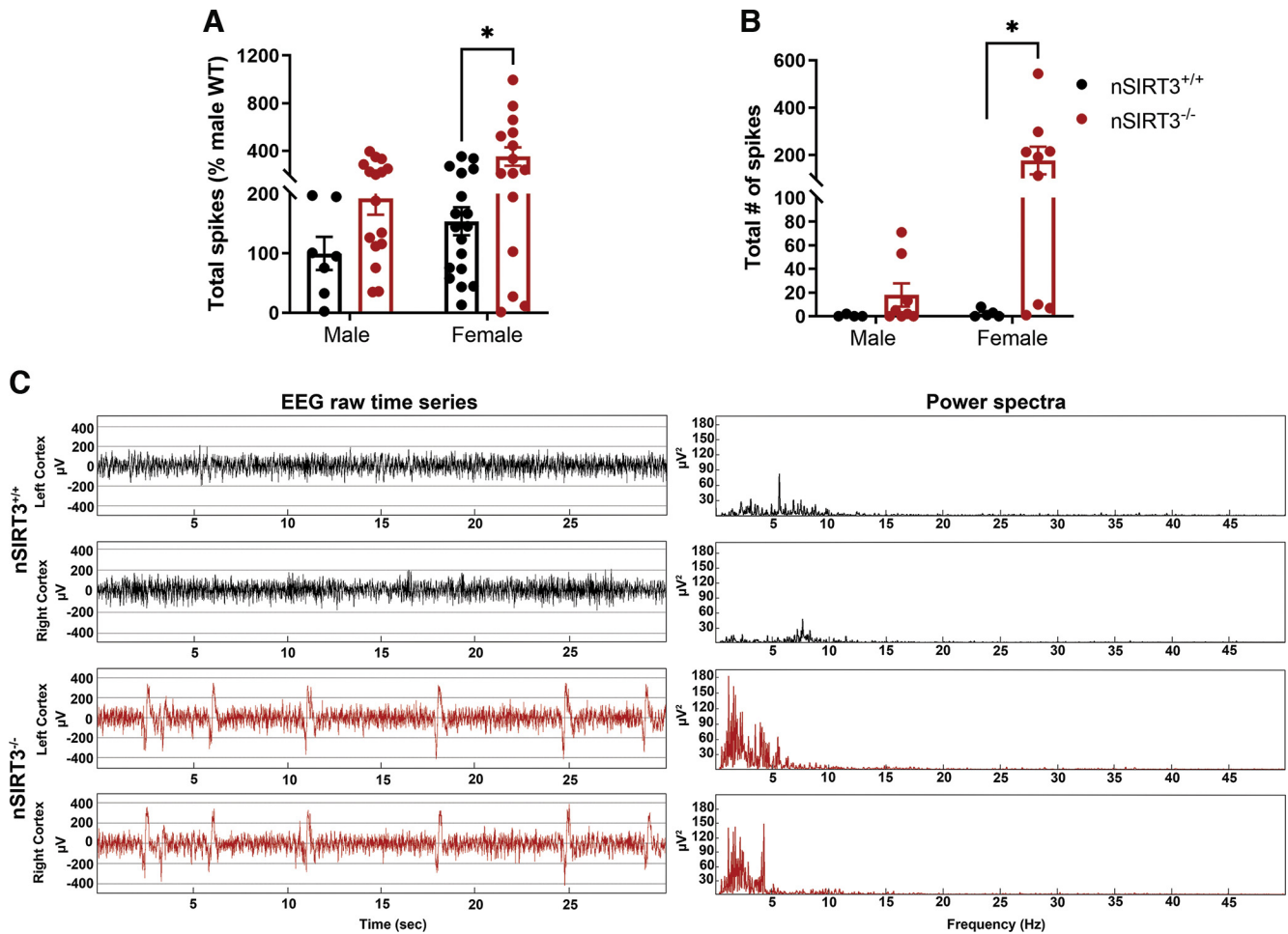


Figure 5. Neuronal deletion of SIRT3 results in female-specific altered neuronal excitability. **A**, Baseline neuronal spiking in an *in vitro* MEA. Synapse maturity at DIV 9 was verified by coexpression of Synapsin I and NeuN (Extended Data Fig. 5-1). **B**, *In vivo* EEG assessment of spikes over a 2 week period in 12-month-old mice ($n = 5-12/\text{group}$). **C**, Representative trace of interictal spiking in 12-month-old female nSIRT3^{-/-} and nSIRT3^{+/+} mice illustrated in the 30 s time series (left column) and power spectral plots of the corresponding data segments (right column) for both hemispheres. * $p < 0.05$ (two-way ANOVA followed by Sidak's multiple comparison test). Error bars indicate mean \pm SEM.

Together, these data suggest that neuronal SIRT3 deficiency increases *in vitro* glycolytic parameters without overt changes to OXPHOS and induces sex-dependent mitochondrial dysfunction.

Neuron-specific SIRT3 deficiency results in female-specific altered neuronal excitability and working spatial memory impairment

Proper neuronal activity depends on tightly regulated metabolic control. To determine whether neuronal-specific SIRT3 deficiency produced functional deficits, we first investigated network excitability by observing baseline neuronal spiking events using an MEA in male and female, nSIRT3^{+/+} and nSIRT3^{-/-} mixed neuronal-glia cultures (DIV 9). The total number of spikes recorded over a 30 min period was significantly elevated in female nSIRT3^{-/-} cultures compared with all other groups (Fig. 5A), suggesting a propensity toward neuronal hyperexcitability. Maturity of the cultures was verified by coexpression of Synapsin I and NeuN (Extended Data Fig. 5-1). To determine whether this altered neuronal excitability occurred in adult mice, 12-month-old nSIRT3^{+/+} and nSIRT3^{-/-} mice were implanted with bilateral EEG electrodes located over the motor/somatosensory cortex. Although no spontaneous seizures were detected over the 2 week observation period, sharp waves known as ISs appeared consistently in EEG records obtained from nSIRT3^{-/-} mice on

one or both cortical channels (at least 2 spikes appeared in records obtained from 40% of male nSIRT3^{+/+} mice, 16.6% of female nSIRT3^{+/+} mice, 60% of male nSIRT3^{-/-} mice, and 66.7% of female nSIRT3^{-/-} mice). Neuronal spikes are generated by the sudden, synchronous discharge of groups of neurons and are considered a biomarker of hyperexcitability and epilepsy (for review, see Staley and Dudek, 2006). The total number of sharp discharges at least $3\times$ baseline on one or both cortical channels was highly variable within groups but corroborated our *in vitro* findings of increased excitability in nSIRT3^{-/-} mice with a tendency for increased spiking in female nSIRT3^{-/-} mice (Fig. 5B). Representative traces of interictal spiking and power spectral plot of the corresponding 30 s data segment in 12-month-old female nSIRT3^{-/-} and nSIRT3^{+/+} are illustrated in Figure 5C. Together, these data demonstrate that neuron-specific SIRT3 deficiency results in altered neuronal excitability in female mice.

To probe cognitive function, short-term working spatial memory was assessed using the spontaneous alternation version of the Y-maze task. Female nSIRT3^{-/-} mice exhibited significantly reduced correct spontaneous alternations at 6 months (Fig. 6A), 12 months (Fig. 6B), and in inducible SIRT3 KO (*Camk2^{cre}/ERT2*) mice (Fig. 6C). These deficits were not accompanied by differences in locomotion, as measured by total arm entries (Fig. 6D,E), indicating that neuronal SIRT3 deficiency is

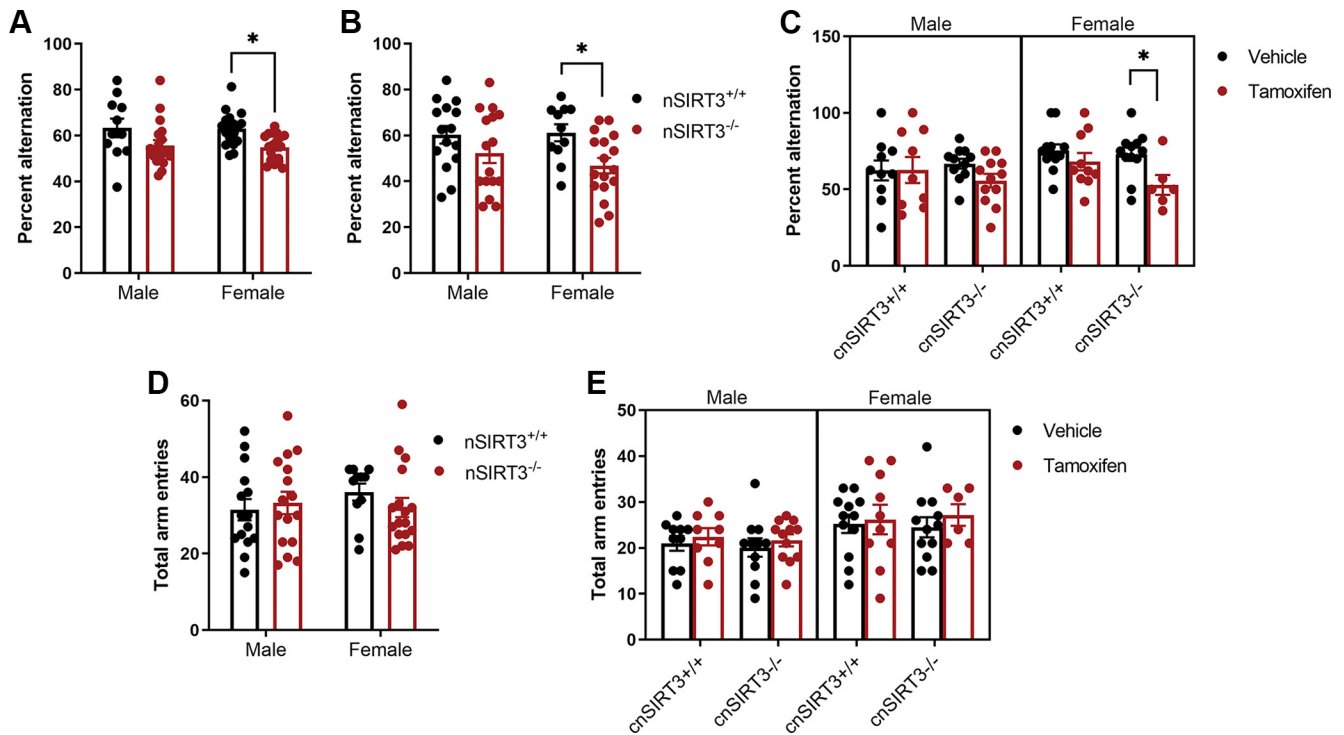


Figure 6. Neuronal deletion of SIRT3 results in female-specific working spatial memory impairment. Y-maze assessment of spatial working memory in mice at (A) 6 months of age ($n = 11$ – 19 /group, 2 cohorts), (B) 12 months of age ($n = 11$ – 17 /group, 3 cohorts), and (C) on inducible neuronal SIRT3 deletion ($n = 6$ – 12 /group, 4 cohorts). Locomotion assessment, measured by total arm entries in mice at (D) 12 months of age ($n = 11$ – 17 /group) and (E) on inducible neuronal SIRT3 deletion ($n = 6$ – 12 /group, 4 cohorts). * $p < 0.05$ (two-way ANOVA followed by Sidak's multiple comparison test). Error bars indicate mean \pm SEM.

capable of inducing working spatial memory impairment in female mice, specifically.

Discussion

Increasing evidence suggests that SIRT3 functions in a complex and context-dependent manner to influence health and disease. Outright metabolic dysfunction in germline SIRT3^{-/-} mice occurs only after an additional insult, such as fasting or high-fat diet, leading to the general consensus that SIRT3 functions as a mitochondrial stress sensor (Ahn et al., 2008; Sundaresan et al., 2009; Hirschey et al., 2010; Qiu et al., 2010; Someya et al., 2010; Hirschey et al., 2011; Fernandez-Marcos et al., 2012; Tyagi et al., 2018). Thus, it appears that SIRT3 dysfunction per se is not sufficient to drive pathology perhaps because of compensatory effects. Importantly, most studies in SIRT3 KO mice have reported data comprised mostly or entirely of male mice. Here, we demonstrate that targeted SIRT3 deletion in select neurons of the neocortex and hippocampus, preferentially predisposes female mice to differential protein acetylation, increased cortical O₂⁻ levels, altered neuronal excitability, and working spatial memory deficits. This would suggest that SIRT3 deficiency and resultant SOD2 acetylation at lysine site K122 hyperacetylation exerts sexually dimorphic effects on metabolic function. Moreover, data from this study suggest that neuronal deletion of SIRT3 is sufficient to drive dysfunction in females but not in males. Importantly, the data presented here implicate a novel mechanism by which sex differences can arise in aging and neurologic disease.

Mitochondria have evolved to respond to changes in energy demand. Reversible acetylation/deacetylation of proteins provides one such mechanism to rapidly alter mitochondrial function in response to redox state and/or energy demand. In line

with its role as the primary mitochondrial deacetylase, germline and cell type-specific deletion of SIRT3 in mice consistently increases mitochondrial protein acetylation (Lombard et al., 2007; Hirschey et al., 2010, 2011; Fernandez-Marcos et al., 2012; Dittenhafer-Reed et al., 2015; Cheng et al., 2016; Tyagi et al., 2018; Nandi et al., 2019). Likewise, our neuron-specific SIRT3 deletion resulted in significant cortical mitochondrial acetylation albeit with fewer identified acetylated sites than previous studies, likely owing to the presence of functional SIRT3 in glia, oligodendrocytes, and other neuronal populations in our study. Like other acetylomic analyses, the majority of the hyperacetylated proteins identified were involved in core metabolic processes, such as the TCA cycle and OXPHOS (Dittenhafer-Reed et al., 2015). Protein immunoblotting revealed significantly increased mitochondrial acetylation in male and female nSIRT3^{-/-} mice, suggesting a unique and persistent effect of reduced SIRT3 activity.

To what degree protein hyperacetylation affects protein activity is largely context-dependent (Fernandez-Marcos et al., 2012). For example, acetylation at one key lysine residue may or may not have greater implications for target protein activity than acetylation at multiple ancillary sites. Here, we identified direct sex-dependent alterations to SOD2 at key functional lysine site K122 (Qiu et al., 2010; Tao et al., 2010; Chen et al., 2011). In addition, we illustrate a female-dependent decrease in SOD2 enzymatic activity, suggesting that acetylation at K122, at least in neurons, is sufficient to affect SOD2 activity in female mice. Similarly, we identified hyperacetylation of known SIRT3 targets, aconitase and CI subunits. Examination of the activity of these proteins in nSIRT3^{-/-} mice revealed that hyperacetylation did not alter CI, aconitase, and fumarase activity, regardless of sex. Hyperacetylation of mitochondrial proteins, under most circumstances, leads to inhibition of

target protein activity (Schlicker et al., 2008). Aconitase is one protein whose activity has been shown to increase on hyperacetylation (Fernandes et al., 2015). Conversely, the iron-sulfur core of aconitase is sensitive to specific oxidation by O_2^- , which is associated with decreased enzymatic activity (Gardner et al., 1995; Patel et al., 1996). Increased O_2^- levels in female nSIRT3^{-/-} mice could offset any alterations to aconitase activity induced by hyperacetylation. Thus, here we show that, despite differences in protein acetylation between the sexes, the indirect effects of these major SIRT3 target protein activities are unaffected by biological sex.

CI and SOD2 are robust mitochondrial enzymes, and slight inhibition of activity is not necessarily sufficient to diminish function. CI provides ~40% of the proton-motive force required for cellular respiration and is also the primary site of O_2^- production (Giachin et al., 2016). As a potential dual threat in the highly oxidant-vulnerable brain, CI function is tightly regulated in an activity-dependent manner. Nonsynaptic mitochondria can withstand upwards of 70% depletion of CI activity before a decrease in oxygen consumption (OC) is observed, whereas inhibition of CI activity by as little as 10% is sufficient to impair OC in synaptic mitochondria (Davey et al., 1997, 1998). Here, despite our reported absence of change in CI activity in both male and female nSIRT3^{-/-} mice, only female nSIRT3^{-/-} mitochondria exhibited significantly impaired OC and elevated O_2^- levels. Electron flow through CII stimulated by succinate addition was unable to correct deficient OXPHOS in female nSIRT3^{-/-} mice leading to a trend toward overall decreased maximum respiratory capacity. CI is a well-known source of intracellular O_2^- . Deficits in CI could contribute additional electrons to the formation of O_2^- by electron leak through CI and may be sufficient to create a vicious cycle of O_2^- driven O_2^- production in female nSIRT3^{-/-} mice. The observed increase in glycolysis in primary cultures from female nSIRT3^{-/-} mice may be indicative of shunting to bypass CI dysfunction and/or to minimize ROS production. On the other hand, this could provide further evidence of aberrant glucose metabolism, which may be attributed to the indirect effects of mitochondrial protein acetylation. Nonetheless, this demonstrates that neuronal-specific SIRT3 deletion induces sexually divergent effects on mitochondrial function, rendering females more vulnerable to metabolic dysfunction and oxidative stress.

Mitochondrial dysfunction and oxidative stress have been implicated as key factors underlying cognitive aging and neurodegenerative disease (Kapogiannis and Mattson, 2011; Johri and Beal, 2012; Joseph et al., 2012; Giachin et al., 2016; Shi et al., 2017). Yet, the role of sirtuins in cognitive aging and cognition more generally is only beginning to emerge (Satoh et al., 2017; Diaz-Perdigon et al., 2020). We provide evidence that female nSIRT3^{-/-} mice exhibit deficits in spatial working memory. Spatial working memory is the ability to keep information active for recall over short periods and is mediated primarily by cortical and hippocampal areas of the brain, regions that exhibited decreased SIRT3 expression in our model (van Asselen et al., 2006). Notably, impairment of working memory is highly affected by the aging process and one of earliest predictors of AD (Dobbs and Rule, 1989; Baddeley et al., 1991; Kirova et al., 2015; Cansino et al., 2020). We observed sex-specific deficits in female nSIRT3^{-/-} mice regardless of age. Moreover, we were able to replicate this sex-specific deficit in spatial working memory on inducible deletion of SIRT3 in adult mice. This suggests that SIRT3 deficiency selectively predisposes female mice to deficits in

working memory. In this regard, our data are consistent with the literature in that male nSIRT3^{-/-} mice are relatively unremarkable under normal circumstances. Thus, we are the first to report deficits in memory function as a specific result of neuronal-SIRT3 deletion. Further, these effects were present despite functional SIRT3 in other neuronal and non-neuronal cells in the brain, implicating a particular dependency of forebrain neurons on functional SIRT3. Cortical and hippocampal neurons generally exhibit increased activity and metabolism relative to other brain regions and therefore may be vulnerable to not only AD-related pathology but to the loss of SIRT3 (Buckner et al., 2009).

Further, we show that both *in vitro* and *in vivo* female nSIRT3^{-/-} mice exhibit increased baseline neuronal excitability relative to all other groups, a finding that adds to the growing literature suggesting a role for sirtuins in neuronal hyperexcitability and seizures (Wang et al., 2016; Hall et al., 2017). We have previously demonstrated SIRT3 dysfunction in a male rat model of temporal lobe epilepsy (Gano et al., 2018). Neuronal-specific deletion of the SIRT3 downstream effector, SOD2, is sufficient to produce a catastrophic epilepsy (Fulton et al., 2021). Additionally, SIRT3 haploinsufficiency when combined with an AD mouse model exacerbates neuronal spiking and seizure incidence in a GABA-dependent manner (Cheng et al., 2020). Although spontaneous seizures were not detected in the 2 week observation period, interictal spiking was observed. Increased neuronal excitability puts an additional metabolic stress on cellular respiration and likely contributes to the observed female-specific O_2^- levels. Increased O_2^- can cause further oxidative damage to core ETC components, thus engaging female nSIRT3^{-/-} mice in a feedforward cycle that may lead to synaptic dysfunction.

While neuronal spiking was reported in primary cultures derived from nSIRT3^{+/+} and nSIRT3^{-/-} mice using MEA recordings and further confirmed *in vivo* using video-EEG, a limitation of this study is that additional experiments, such as seizure threshold tests to measure hyperexcitability, would be needed to validate a hyperexcitability phenotype. In addition, IS analysis would have been further refined by the inclusion of hippocampal and electromyogram recordings (Gureviciene et al., 2019).

In conclusion, we demonstrate that neuronal-specific deletion of SIRT3 is sufficient to drive sex differences in brain metabolism, altered neuronal excitability, and cognitive function. This work provides a model by which female-specific deficits resulting from mitochondrial dysfunction might arise in aging and neurologic disease.

References

- Ahn BH, Kim HS, Song S, Lee IH, Liu J, Vassilopoulos A, Deng CX, Finkel T (2008) A role for the mitochondrial deacetylase Sirt3 in regulating energy homeostasis. *Proc Natl Acad Sci USA* 105:14447–14452.
- Ali HR, Assiri MA, Harris PS, Michel CR, Yun Y, Marentette JO, Huynh FK, Orlicky DJ, Shearn CT, Saba LM, Reisdorph R, Reisdorph N, Hirschey MD, Fritz KS (2019) Quantifying competition among mitochondrial protein acylation events induced by ethanol metabolism. *J Proteome Res* 18:1513–1531.
- Assiri MA, Roy SR, Harris PS, Ali H, Liang Y, Shearn CT, Orlicky DJ, Roede JR, Hirschey MD, Backos DS, Fritz KS (2017) Chronic ethanol metabolism inhibits hepatic mitochondrial superoxide dismutase via lysine acetylation. *Alcohol Clin Exp Res* 41:1705–1714.
- Austad SN (2011) Sex differences in longevity and aging. In: *Handbook of the biology of aging* (Masoro EJ, Austad SN, eds), Ed 7. San Diego: Academic.

- Baddeley AD, Bressi S, Della Sala S, Logie R, Spinnler H (1991) The decline of working memory in Alzheimer's disease: a longitudinal study. *Brain* 114:2521–2542.
- Bellizzi D, Rose G, Cavalcante P, Covello G, Dato S, De Rango F, Greco V, Maggiolini M, Feraco E, Mari V, Franceschi C, Passarino G, De Benedictis G (2005) A novel VNTR enhancer within the SIRT3 gene, a human homologue of SIR2, is associated with survival at oldest ages. *Genomics* 85:258–263.
- Bellizzi D, Dato S, Cavalcante P, Covello G, Di Cianni F, Passarino G, Rose G, De Benedictis G (2007) Characterization of a bidirectional promoter shared between two human genes related to aging: SIRT3 and PSMD13. *Genomics* 89:143–150.
- Birch-Machin MA, Turnbull DM (2001) Assaying mitochondrial respiratory complex activity in mitochondria isolated from human cells and tissues. *Methods Cell Biol* 65:97–117.
- Buckner RL, Sepulcre J, Talukdar T, Krienen FM, Liu H, Hedden T, Andrews-Hanna JR, Sperling RA, Johnson KA (2009) Cortical hubs revealed by intrinsic functional connectivity: mapping, assessment of stability, and relation to Alzheimer's disease. *J Neurosci* 29:1860–1873.
- Cansino S, Torres-Trejo F, Estrada-Manilla C, Pérez-Loyda M, Ramírez-Barajas L, Hernández-Ladrón-deGuevara M, Nava-Chaparro A, Ruiz-Velasco S (2020) Predictors of working memory maintenance and decline in older adults. *Arch Gerontol Geriatr* 89:104074.
- Chen Y, Zhang J, Lin Y, Lei Q, Guan KL, Zhao S, Xiong Y (2011) Tumour suppressor SIRT3 deacetylates and activates manganese superoxide dismutase to scavenge ROS. *EMBO Rep* 12:534–541.
- Cheng A, Yang Y, Zhou Y, Maharana C, Lu D, Peng W, Liu Y, Wan R, Marosi K, Misiak M, Bohr VA, Mattson MP (2016) Mitochondrial SIRT3 mediates adaptive responses of neurons to exercise and metabolic and excitatory challenges. *Cell Metab* 23:128–142.
- Cheng A, Wang J, Ghena N, Zhao Q, Perone I, King TM, Veech RL, Gorospe M, Wan R, Mattson MP (2020) SIRT3 haploinsufficiency aggravates loss of GABAergic interneurons and neuronal network hyperexcitability in an Alzheimer's disease model. *J Neurosci* 40:694.
- Davey GP, Canevari L, Clark JB (1997) Threshold effects in synaptosomal and nonsynaptic mitochondria from hippocampal CA1 and paramedian neocortex brain regions. *J Neurochem* 69:2564–2570.
- Davey GP, Peuchen S, Clark JB (1998) Energy thresholds in brain mitochondria: potential involvement in neurodegeneration. *J Biol Chem* 273:12753–12757.
- Diaz-Perdigon T, Belloch FB, Ricobaraza A, Elboray EE, Suzuki T, Tordera RM, Puerta E (2020) Early sirtuin 2 inhibition prevents age-related cognitive decline in a senescence-accelerated mouse model. *Neuropsychopharmacology* 45:347–357.
- Dikalova AE, Itani HA, Nazarewicz RR, McMaster WG, Flynn CR, Uzhachenko R, Fessel JP, Gamboa JL, Harrison DG, Dikalov SI (2017) Sirt3 impairment and SOD2 hyperacetylation in vascular oxidative stress and hypertension. *Circ Res* 121:564–574.
- Dittenhafer-Reed KE, Richards AL, Fan J, Smallegan MJ, Fotuhi Siahpirani A, Kemmerer ZA, Prolla TA, Roy S, Coon JJ, Denu JM (2015) SIRT3 mediates multi-tissue coupling for metabolic fuel switching. *Cell Metab* 21:637–646.
- Dobbs AR, Rule BG (1989) Adult age differences in working memory. *Psychol Aging* 4:500–503.
- Fernandes J, Weddle A, Kinter CS, Humphries KM, Mather T, Szweda LI, Kinter M (2015) Lysine acetylation activates mitochondrial aconitase in the heart. *Biochemistry* 54:4008–4018.
- Fernandez-Marcos PJ, Jeninga EH, Canto C, Harach T, de Boer VC, Andreux P, Moullan N, Pirinen E, Yamamoto H, Houten SM, Schoonjans K, Auwerx J (2012) Muscle or liver-specific Sirt3 deficiency induces hyperacetylation of mitochondrial proteins without affecting global metabolic homeostasis. *Sci Rep* 2:425.
- Fink B, Laude K, McCann L, Doughan A, Harrison DG, Dikalov S (2004) Detection of intracellular superoxide formation in endothelial cells and intact tissues using dihydroethidium and an HPLC-based assay. *Am J Physiol Cell Physiol* 287:C895–C902.
- Finley LW, Haigis MC (2012) Metabolic regulation by SIRT3: implications for tumorigenesis. *Trends Mol Med* 18:516–523.
- Finnin MS, Donigian JR, Pavletich NP (2001) Structure of the histone deacetylase SIRT2. *Nat Struct Biol* 8:621–625.
- Flurkey K, Currer JM, Harrison DE (2007) Mouse models in aging research. In: *The mouse in biomedical research* (Fox JG, Davisson MT, Quimby FW, Barthold SW, Newcomer CE, Smith AL, eds), Ed 2. San Diego: Academic.
- Fulton RE, Pearson-Smith JN, Huynh CQ, Fabisiak T, Liang LP, Aivazidis S, High BA, Buscaglia G, Corrigan T, Valdez R, Shimizu T, Patel MN (2021) Neuro-specific mitochondrial oxidative stress results in epilepsy, glucose dysregulation and a striking astrocyte response. *Neurobiol Dis* 158:105470.
- Gano LB, Liang LP, Ryan K, Michel CR, Gomez J, Vassilopoulos A, Reisdorph N, Fritz KS, Patel M (2018) Altered mitochondrial acetylation profiles in a kainic acid model of temporal lobe epilepsy. *Free Radic Biol Med* 123:116–124.
- Gardner PR, Raineri I, Epstein LB, White CW (1995) Superoxide radical and iron modulate aconitase activity in mammalian cells. *J Biol Chem* 270:13399–13405.
- Garland PB, Shepherd D, Yates DW (1965) Steady-state concentrations of coenzyme A, acetyl-coenzyme A and long-chain fatty acyl-coenzyme A in rat-liver mitochondria oxidizing palmitate. *Biochem J* 97:587–594.
- Giachin G, Bouverot R, Acajjaoui S, Pantalone S, Soler-López M (2016) Dynamics of human mitochondrial complex I assembly: implications for neurodegenerative diseases. *Front Mol Biosci* 3:43.
- Goebbels S, Bormuth I, Bode U, Hermanson O, Schwab MH, Nave KA (2006) Genetic targeting of principal neurons in neocortex and hippocampus of NEX-Cre mice. *Genesis* 44:611–621.
- Gureviciene I, Ishchenko I, Ziyatdinova S, Jin N, Lipponen A, Gurevicius K, Tanila H (2019) Characterization of epileptic spiking associated with brain amyloidosis in APP/PS1 mice. *Front Neurol* 10:1151.
- Hall AM, Brennan GP, Nguyen TM, Singh-Taylor A, Mun HS, Sargious MJ, Baram TZ (2017) The role of Sirt1 in epileptogenesis. *eNeuro* 4:ENEURO.0301-16.2017.
- Herculano-Houzel S (2014) The glia/neuron ratio: how it varies uniformly across brain structures and species and what that means for brain physiology and evolution. *Glia* 62:1377–1391.
- Hirschey MD, Shimazu T, Goetzman E, Jing E, Schwer B, Lombard DB, Grueter CA, Harris C, Biddinger S, Ilkayeva OR, Stevens RD, Li Y, Saha AK, Ruderman NB, Bain JR, Newgard CB, Farese RV Jr, Alt FW, Kahn CR, Verdin E (2010) SIRT3 regulates mitochondrial fatty-acid oxidation by reversible enzyme deacetylation. *Nature* 464:121–125.
- Hirschey MD, et al. (2011) SIRT3 deficiency and mitochondrial protein hyperacetylation accelerate the development of the metabolic syndrome. *Mol Cell* 44:177–190.
- Jin L, Galonek H, Israelian K, Choy W, Morrison M, Xia Y, Wang X, Xu Y, Yang Y, Smith JJ, Hoffmann E, Carney DP, Perni RB, Jirousek MR, Bemis JE, Milne JC, Sinclair DA, Westphal CH (2009) Biochemical characterization, localization, and tissue distribution of the longer form of mouse SIRT3. *Protein Sci* 18:514–525.
- Johri A, Beal MF (2012) Mitochondrial dysfunction in neurodegenerative diseases. *J Pharmacol Exp Ther* 342:619–630.
- Joseph AM, Adhithetty PJ, Buford TW, Wohlgenuth SE, Lees HA, Nguyen LM, Aranda JM, Sandesara BD, Pahor M, Manini TM, Marzetti E, Leeuwenburgh C (2012) The impact of aging on mitochondrial function and biogenesis pathways in skeletal muscle of sedentary high- and low-functioning elderly individuals. *Aging Cell* 11:801–809.
- Kaeberlein M, McVey M, Guarente L (1999) The SIR2/3/4 complex and SIR2 alone promote longevity in *Saccharomyces cerevisiae* by two different mechanisms. *Genes Dev* 13:2570–2580.
- Kapogiannis D, Mattson MP (2011) Disrupted energy metabolism and neuronal circuit dysfunction in cognitive impairment and Alzheimer's disease. *Lancet Neurol* 10:187–198.
- Kim SC, Sprung R, Chen Y, Xu Y, Ball H, Pei J, Cheng T, Kho Y, Xiao H, Xiao L, Grishin NV, White M, Yang XJ, Zhao Y (2006) Substrate and functional diversity of lysine acetylation revealed by a proteomics survey. *Mol Cell* 23:607–618.
- Kirova AM, Bays RB, Lagalwar S (2015) Working memory and executive function decline across normal aging, mild cognitive impairment, and Alzheimer's disease. *Biomed Res Int* 2015:748212.
- Kumar S, Lombard DB (2015) Mitochondrial sirtuins and their relationships with metabolic disease and cancer. *Antioxid Redox Signal* 22:1060–1077.
- Liang LP, Patel M (2006) Seizure-induced changes in mitochondrial redox status. *Free Radic Biol Med* 40:316–322.
- Lombard DB, Alt FW, Cheng HL, Bunkenborg J, Streeper RS, Mostoslavsky R, Kim J, Yancopoulos G, Valenzuela D, Murphy A, Yang Y, Chen Y, Hirschey MD, Bronson RT, Haigis M, Guarente LP, Farese RV,

- Weissman S, Verdin E, Schwer B (2007) Mammalian Sir2 homolog SIRT3 regulates global mitochondrial lysine acetylation. *Mol Cell Biol* 27:8807–8814.
- Madisen L, Zwingman TA, Sunkin SM, Oh SW, Zariwala HA, Gu H, Ng LL, Palmiter RD, Hawrylycz MJ, Jones AR, Lein ES, Zeng H (2010) A robust and high-throughput Cre reporting and characterization system for the whole mouse brain. *Nat Neurosci* 13:133–140.
- Maghzal GJ, Stocker R (2007) Improved analysis of hydroethidine and 2-hydroxyethidium by HPLC and electrochemical detection. *Free Radic Biol Med* 43:1095–1096.
- McConnell ER, McClain MA, Ross J, Lefew WR, Shafer TJ (2012) Evaluation of multi-well microelectrode arrays for neurotoxicity screening using a chemical training set. *Neurotoxicology* 33:1048–1057.
- McLean AC, Valenzuela N, Fai S, Bennett SA (2012) Performing vaginal lavage, crystal violet staining, and vaginal cytological evaluation for mouse estrous cycle staging identification. *J Vis Exp* 67:e4389.
- Nandi SK, Nahomi RB, Harris PS, Michel CR, Fritz KS, Nagaraj RH (2019) The absence of SIRT3 and SIRT5 promotes the acetylation of lens proteins and improves the chaperone activity of α -crystallin in mouse lenses. *Exp Eye Res* 182:1–9.
- Onyango P, Celic I, McCaffery JM, Boeke JD, Feinberg AP (2002) SIRT3, a human SIR2 homologue, is an NAD-dependent deacetylase localized to mitochondria. *Proc Natl Acad Sci USA* 99:13653–13658.
- Patel M, Day BJ, Crapo JD, Fridovich I, McNamara JO (1996) Requirement for superoxide in excitotoxic cell death. *Neuron* 16:345–355.
- Pelletier M, Billingham LK, Ramaswamy M, Siegel RM (2014) Extracellular flux analysis to monitor glycolytic rates and mitochondrial oxygen consumption. In: *Methods in enzymology* (Galluzzi L, Kroemer G, eds). San Diego: Academic.
- Pukhalskaia AE, Dyatlova AS, Linkova NS, Kozlov KL, Kvetnaia TV, Koroleva MV, Kvetnoy IM (2020) Sirtuins as possible predictors of aging and Alzheimer's disease development: verification in the hippocampus and saliva. *Bull Exp Biol Med* 169:821–824.
- Qiu X, Brown K, Hirschey MD, Verdin E, Chen D (2010) Calorie restriction reduces oxidative stress by SIRT3-mediated SOD2 activation. *Cell Metab* 12:662–667.
- Rose G, Dato S, Altomare K, Bellizzi D, Garasto S, Greco V, Passarino G, Feraco E, Mari V, Barbi C, BonaFe M, Franceschi C, Tan Q, Boiko S, Yashin AI, De Benedictis G (2003) Variability of the SIRT3 gene, human silent information regulator Sir2 homologue, and survivorship in the elderly. *Exp Gerontol* 38:1065–1070.
- Satoh A, Imai SI, Guarente L (2017) The brain, sirtuins, and ageing. *Nat Rev Neurosci* 18:362–374.
- Schlicker C, Gertz M, Papatheodorou P, Kachholz B, Becker CF, Steegborn C (2008) Substrates and regulation mechanisms for the human mitochondrial sirtuins Sirt3 and Sirt5. *J Mol Biol* 382:790–801.
- Shi H, Deng HX, Gius D, Schumacker PT, Surmeier DJ, Ma YC (2017) Sirt3 protects dopaminergic neurons from mitochondrial oxidative stress. *Hum Mol Genet* 26:1915–1926.
- Someya S, Yu W, Hallows WC, Xu J, Vann JM, Leeuwenburgh C, Tanokura M, Denu JM, Prolla TA (2010) Sirt3 mediates reduction of oxidative damage and prevention of age-related hearing loss under caloric restriction. *Cell* 143:802–812.
- Staley KJ, Dudek FE (2006) Interictal spikes and epileptogenesis. *Epilepsy Curr* 6:199–202.
- Sun Y, Oberley LW, Li Y (1988) A simple method for clinical assay of superoxide dismutase. *Clin Chem* 34:497–500.
- Sundaresan NR, Gupta M, Kim G, Rajamohan SB, Isbatan A, Gupta MP (2009) Sirt3 blocks the cardiac hypertrophic response by augmenting Foxo3a-dependent antioxidant defense mechanisms in mice. *J Clin Invest* 119:2758–2771.
- Tao R, Coleman MC, Pennington JD, Ozden O, Park SH, Jiang H, Kim HS, Flynn CR, Hill S, Hayes McDonald W, Olivier AK, Spitz DR, Gius D (2010) Sirt3-mediated deacetylation of evolutionarily conserved lysine 122 regulates MnSOD activity in response to stress. *Mol Cell* 40:893–904.
- Tyagi A, Nguyen CU, Chong T, Michel CR, Fritz KS, Reisdorph N, Knaub L, Reusch JE, Pugazhenti S (2018) SIRT3 deficiency-induced mitochondrial dysfunction and inflammasome formation in the brain. *Sci Rep* 8:17547.
- van Asselen M, Kessels RP, Neggers SF, Kappelle LJ, Frijns CJ, Postma A (2006) Brain areas involved in spatial working memory. *Neuropsychologia* 44:1185–1194.
- Verdin E, Ott M (2015) 50 years of protein acetylation: from gene regulation to epigenetics, metabolism and beyond. *Nat Rev Mol Cell Biol* 16:258–264.
- Votion DM, Gnaiger E, Lemieux H, Mouithys-Mickalad A, Serteryn D (2012) Physical fitness and mitochondrial respiratory capacity in horse skeletal muscle. *PLoS One* 7:e34890.
- Wagner GR, Bhatt DP, O'Connell TM, Thompson J, Dubois LG, Backos DS, Yang H, Mitchell GA, Ilkayeva OR, Stevens RD, Grimsrud PA, Hirschey MD (2017) A class of reactive Acyl-CoA species reveals the non-enzymatic origins of protein acylation. *Cell Metab* 25:823–837.e8.
- Wang D, Li Z, Zhang Y, Wang G, Wei M, Hu Y, Ma S, Jiang Y, Che N, Wang X, Yao J, Yin J (2016) Targeting of microRNA-199a-5p protects against pilocarpine-induced status epilepticus and seizure damage via SIRT1-p53 cascade. *Epilepsia* 57:706–716.
- Weir HJ, Murray TK, Kehoe PG, Love S, Verdin EM, O'Neill MJ, Lane JD, Balthasar N (2012) CNS SIRT3 expression is altered by reactive oxygen species and in Alzheimer's disease. *PLoS One* 7:e48225.
- Yang W, Nagasawa K, Münch C, Xu Y, Satterstrom K, Jeong S, Hayes SD, Jedrychowski MP, Sejal Vyas F, Zaganjor E, Guarani V, Ringel AE, Gygi SP, Harper JW, Haigis MC (2016) Mitochondrial sirtuin network reveals dynamic SIRT3-dependent deacetylation in response to membrane depolarization. *Cell* 167:985–1000.e21.
- Yin J, Han P, Song M, Nielsen M, Beach TG, Serrano GE, Liang WS, Caselli RJ, Shi J (2018) Amyloid- β increases tau by mediating sirtuin 3 in Alzheimer's disease. *Mol Neurobiol* 55:8592–8601.
- Zhao H, Joseph J, Fales HM, Sokoloski EA, Levine RL, Vasquez-Vivar J, Kalyanaraman B (2005) Detection and characterization of the product of hydroethidine and intracellular superoxide by HPLC and limitations of fluorescence. *Proc Natl Acad Sci USA* 102:5727–5732.
- Zhao H, Kalivendi S, Zhang H, Joseph J, Nithipatikom K, Vásquez-Vivar J, Kalyanaraman B (2003) Superoxide reacts with hydroethidine but forms a fluorescent product that is distinctly different from ethidium: potential implications in intracellular fluorescence detection of superoxide. *Free Radic Biol Med* 34:1359–1368.
- Zielonka J, Vasquez-Vivar J, Kalyanaraman B (2006) The confounding effects of light, sonication, and Mn(III)TBAP on quantitation of superoxide using hydroethidine. *Free Radic Biol Med* 41:1050–1057.